An Ionic Capacitor for Integrated Iontronic Circuits

Per Janson, Erik O. Gabrielsson, Keon Jae Lee, Magnus Berggren,* and Daniel T. Simon

Organic electronics, in combination with custom polyelectrolytes, enables solid- and hydrogel-state circuit components using ionic charges in place of the electrons of traditional electronics. This growing field of iontronics leverages anion- and cation-exchange membranes as analogs to n-type and p-type semiconductors, and conjugated polymer electrodes as ion-to-electron converters. To date, the iontronics toolbox includes ionic resistors, ionic diodes, ionic transistors, and analog and digital circuits comprised thereof. Here, an ionic capacitor based on mixed electron–ion conductors is demonstrated. The ionic capacitor resembles the structure of a conventional electrochemical capacitor that is inverted, with an electronically conducting core and two electrolyte ionic conductors. The device is first verified as a capacitor, and then demonstrated as a smoothing element in an iontronic diode bridge circuit driving an organic electronic ion pump (ionic resistor). The ionic capacitor complements the existing iontronics toolbox, enabling more complex and functional ionic circuits, and will thus have implications in a variety of mixed electron–ion conduction technologies.

Organic electronic materials have emerged as a highly versatile component in a variety of bioelectronic applications.[1–5] In particular, the mixed ion–electronic conductivity of these materials, when composited with tailored polyelectrolytes, defines a material amalgamation that has led to the subfield of iontronics,[6] i.e., components and circuits that process ionic in addition to— or instead of—electronic charge carriers. Iontronics allows us to electronically address and control the processing and delivery of ions. Such technology promises a means to bridge the gaps between technology, biology, and chemistry in a novel manner, in

P. Janson, Dr. E. O. Gabrielsson, Prof. M. Berggren, Dr. D. T. Simon
Laboratory of Organic Electronics
Department of Science and Technology
Linköping University
Norrköping 60174, Sweden
E-mail: magnus.berggren@liu.se
Prof. K. J. Lee
Department of Materials Science and Engineering
Korea Advanced Institute of Science and Technology (KAIST)
291 Daehak-ro, Yuseong-gu, Daejeon 34141, Republic of Korea

The ORCID identification number(s) for the author(s) of this article can be found under https://doi.org/10.1002/admt.201800494.

particular for targeted applications in neurobiology and therapy, precise-controlled synthesis at small dimensions, and for electrochemical devices. The most basic iontronic component is the organic electronic ion pump (OEIP).[7–9] The OEIP takes advantage of the lateral electrophoretic transport of charged substances through cation- or anion-exchange membranes (CEM, or AEM, respectively). This structure allows for the selective transport of biologically relevant ionic substances from a source electrolyte to a target electrolyte; for example, positively charged neurotransmitters are "pumped" through the CEM to the target system, while anions are blocked from being transported from the target electrolyte to the source. As the lateral CEMs and AEMs possess a specific ionic conductivity (and no electrical conductivity), the OEIP is essentially an iontronic resistor separ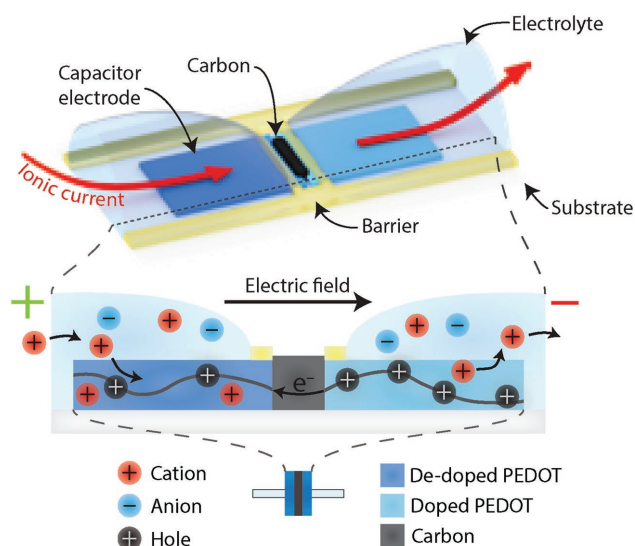ating two electrolytes. Single components and resistive network circuits based on the OEIP have successfully been applied to neurobiology and therapeutic applications, such as for in vitro epilepsy models,[10,11] to achieve modulation of sensory functions in vivo,[12] and to control the pain threshold in awake animals suffering from allodynia.[13]

In addition to iontronic resistors (OEIP), solid-state—or hydrogel-state—iontronic diodes[14–17] and transistors[18] have also been demonstrated and explored in various applications. In these devices, the functionality originates from the accumulation and transport of ions in structures combining CEMs and AEMs. The iontronic diodes and transistors are thus analogous to the device functionality of electronic bipolar devices based on p- and n-type semiconductors. With resistors, diodes, and transistors, a toolbox of iontronic components is at hand. However, capacitive elements are needed to further build advanced circuits for processing of ionic signals, and while ionic capacitors have been demonstrated,[19] they have not yet been integrated into ionic circuits. Here, we present a capacitive device that, in principle, inverts the function of electrochemical supercapacitor in that ionic current flow in its terminals, and the charge is stored internally as electrons that drift between the capacitor terminals. Further, we show the functionality of this iontronic device as a smoothing capacitor in an ionic full wave rectifier circuit.

Poly(3,4-ethylenedioxythiophene) doped with polystyrene sulfonate (PEDOT:PSS) is used, among many other applications, as the electrode material in electrochemical supercapacitors,[20–23] and is known to exhibit significant volumetric capacitance[22,24] and high cyclic stability.[25,26] The capacitive nature of PEDOT:PSS has recently been studied in detail[27,28,29] and found to agree with formation of electric double-layer at

**ADVANCED
SCIENCE NEWS**
www.advancedsciencenews.com

**ADVANCED
MATERIALS
TECHNOLOGIES**
www.advmattechnol.de

Figure 1. Schematic of the ionic capacitor. In the presence of an electric field, the ionic current in the electrolytes is stored in EDLs at the partially doped/de-doped PEDOT:PSS electrodes. The electrodes were 2000 µm wide, 450–2200 µm long, and separated by 800 µm.

Figure 2. Cyclic voltammetry of the ionic capacitor, with A) Scan rates ranging from 25 mV s^{-1} to 200 mV s^{-1} for a device with 4.4 mm^2 electrodes. See Figure S1B in the Supporting Information for additional scan rates up to 800 mV s^{-1}. B) Linearly increasing electrode area (scan rate 50 mV s^{-1}).

the interface between PEDOT and the PSS phase. We propose a design for fully ionic capacitors by simply using two PEDOT:PSS electrodes (mixed ion-electron conduction) connected with carbon (electron conduction only) (**Figure 1**). The two PEDOT:PSS terminals of the ionic capacitors are ionically connected through electrolytes (0.1 M KCl) to either a second pair of (larger) PEDOT:PSS electrodes or to a more complex iontronic circuit.

When a voltage is applied across the device, a current of electrons will pass between the electrodes, and one electrode will be further doped (loss of electrons, polaron formation) and the other partially de-doped. The electronic charge of PEDOT is balanced by ions, and a change in charge is therefore compensated by a flux of ions from (or to) the electrolyte. Consequently, as charge is passed between the electrodes, there is a buildup of electronic and ionic charge at the interfaces between PEDOT and PSS/electrolyte, i.e., formation of electric double-layers (EDLs). Thus, ionic currents in the electrolytes are converted into an electronic current between the electrodes, and ionic and electronic charge is stored in the EDLs (Figure 1). The capacitive nature of the EDLs reduces the current between the electrodes over time, and if the voltage is removed or reversed, the EDLs will discharge through oppositely directed currents.
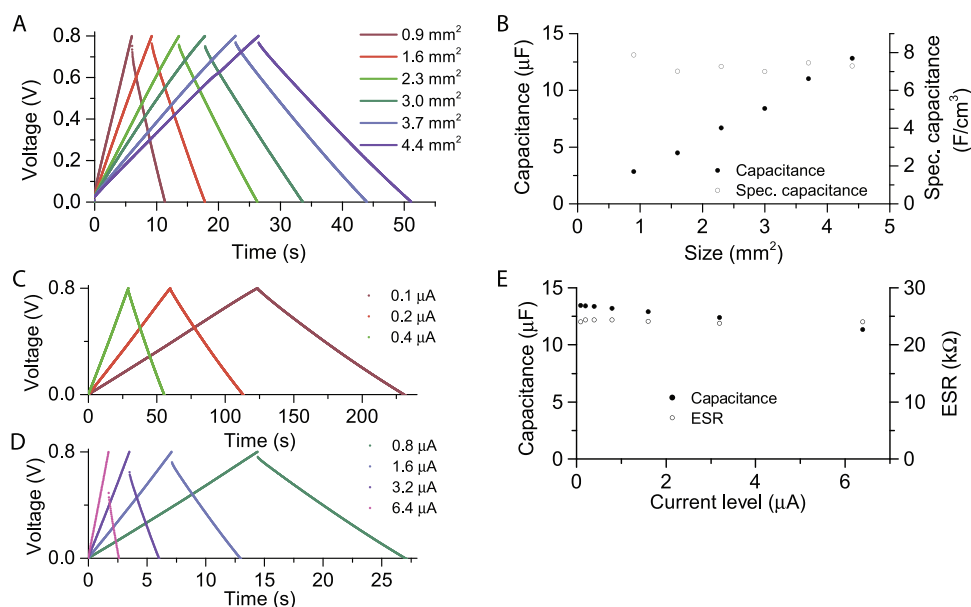
Figure 2A shows the cyclic voltammetry characteristics of the ionic capacitor with 4.4 mm^2 (per side) PEDOT:PSS electrodes, illustrating the hallmark capacitive box for scan rates ranging from 25 to 200 mV s^{-1} and approximately linearly increasing current with scan rate. The corresponding capacitance value is highest, 13.6 µF, for the lowest scan rate, and is reduced to 6.19 µF at 800 mV s^{-1}, see Figure S1A in the Supporting Information. Further, as can be seen in Figure 2B, the current scales linearly with the area of the electrodes (Figure S1C, Supporting Information), giving an average areal capacitance of 290 µF cm^{-2} (at 50 mV s^{-1}), which agrees well with previously published capacitance values for PEDOT:PSS films of this
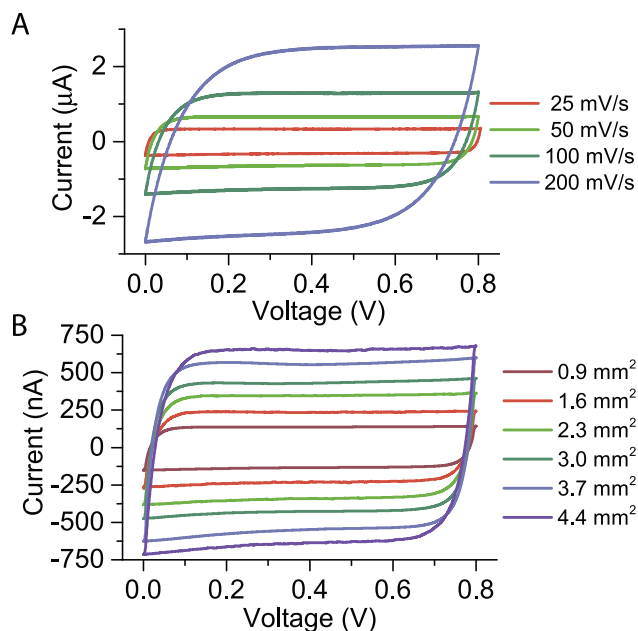
thickness (≈200 nm).[30] In order to avoid electrochemical side-reactions at the electrodes, such as water splitting (Figure S1D, Supporting Information), a maximum voltage of 0.8 V was applied throughout all characterizations. The operational window could potentially be increased by using nonaqueous electrolytes[31]; however, we found the useful voltage window of the design to be ±1 V due to loss of conductivity during de-doping of the electrodes (see Figure S2, Supporting Information).

The charge/discharge characteristics and RC time constant of the ionic capacitor were also investigated. **Figure 3** shows charging at 0.8 V and discharging at 0 V for the capacitor with the largest electrode size (4.4 mm^2). As expected, the evolution of charge and discharge currents follows an exponential behavior,
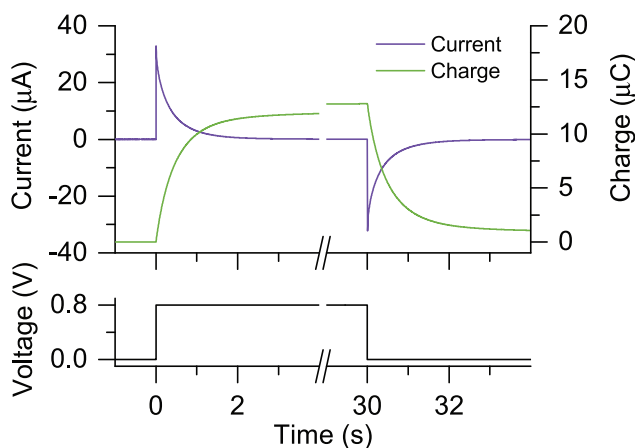
Figure 3. Charge–discharge at +0.8/0 V of the ionic capacitor with 4.4 mm^2 electrode. See Figure S3 in the Supporting Information for charge–discharge at 1 mV pulses.
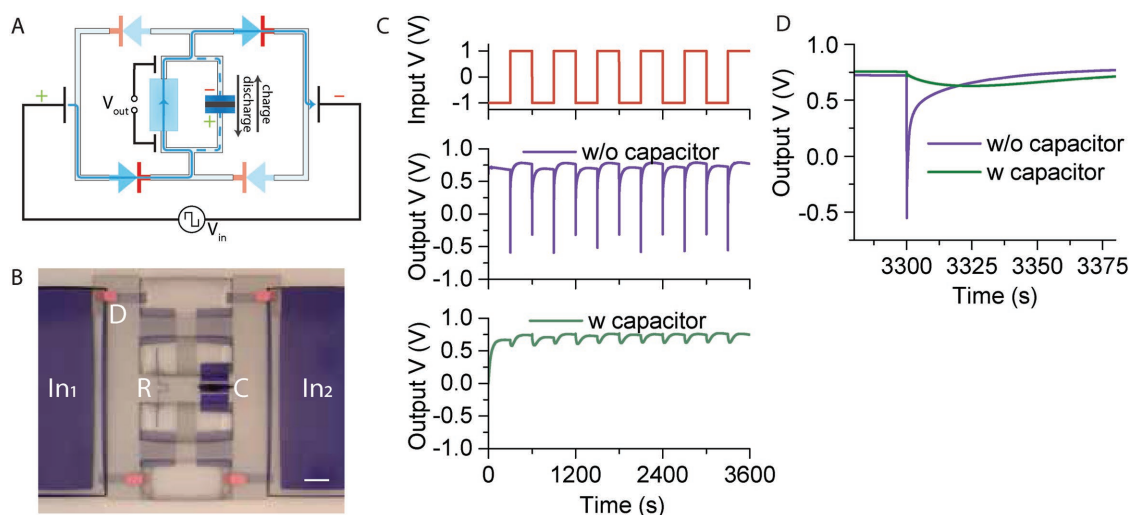
**ADVANCED
SCIENCE NEWS**
www.advancedsciencenews.com

**ADVANCED
MATERIALS
TECHNOLOGIES**
www.advmattechnol.de

Figure 4. Galvanostatic charge–discharge of the ionic capacitor. A) Charge–discharge at ±0.4 µA versus electrode size. B) Capacitance versus electrode size. Capacitance (*C*) was calculated from $C = \frac{i}{\Delta\phi/\Delta t}$, where *i* is the current level and $\Delta\phi/\Delta t$ the slope of the discharge curve. C,D) Charge–discharge versus current level (4.4 mm² electrode area). E) Calculated capacitance and ESR versus current level. See Figure S4B in the Supporting Information for calculated capacitance versus voltage.

with a corresponding time constant of 258 ms. Importantly, the time constant is well below the switch speed of current iontronic bipolar membrane diodes[32] and transistors[33] of similar dimensions as the ionic capacitor, and should thus not limit the overall speed of circuits combining iontronic diodes and transistors with ionic capacitors. In the charged state (at +0.8 V) the current does not completely reach zero, but instead stabilizes around 20 nA. This nonzero current is likely due to side-reactions at the electrodes, which also explains why all charges inserted into the capacitor are not fully recovered during discharge (Figure 3).

The charge and discharge of the ionic capacitor was studied under galvanostatic conditions by charging the device at 0.4 µA up to 0.8 V, followed by discharging at −0.4 µA back to 0 V (**Figure** 4A). The discharge of the capacitor shows a linear change in voltage, and a capacitance that scales linearly with the electrode area (Figure 4B). The capacitance and equivalent series resistance (ESR), were further investigated for the largest electrode configuration for increasing charging currents (0.1–6.4 µA, 0.057–3.6 A cm⁻³ total electrode volume, see Figure 4C,D). Similar to what is typically observed in electrochemical supercapacitors, the capacitance decreases with the magnitude of the charging current from 13.4 to 11.3 µF (Figure 4E). The concentration of ions near the electrodes will decrease with increasing current level, and the capacitance can thus be limited by ion diffusion into the depleted region.[31] The ESR, calculated from the voltage drop which is present as the polarity is changed (Figure S4A, Supporting Information), and is not dependent on the charging current and on average 24.1 ± 0.2 kΩ (Figure 4E). A first-order approximation shows that this measured resistance value is in the same range as the resistance of the electrolytes (54 kΩ, see Supporting Information). The largest electrode configuration was also cycled over an extended period of time at 0.4 µA in order to identify any

degradation in performance (Figure S4C,D, Supporting Information). From this we can conclude that the device lifetime is primarily limited, in its present configuration, by evaporation of the exposed aqueous electrolytes (electrolyte volume ≈20 µL).

With the ionic capacitor characterised, we proceeded to demonstrate its utility in an iontronic diode bridge.[34] The iontronic diode bridge consists of four ionic bipolar membrane diodes,[15–17] each conducting an ionic current when biased in the forward direction but blocking when reversely biased (Figure S5A, Supporting Information). In its basic function, the iontronic diode bridge mimics the characteristics of its electronic counterpart. There are two possible current paths in an ideal diode bridge, where the current flows through one pair of forward-biased diodes and is blocked by the other pair of reversely biased diodes (**Figure** 5A). Regardless of which pair of diodes that conducts, the direction of the current path at the output terminals is the same. In this way, an oscillatory current applied to the input terminals becomes "full-wave" rectified when recorded at the output terminals of the bridge circuit. Unlike electronic diodes, where the carriers can recombine, ionic bipolar membrane diodes exhibit accumulation of mobile ions under forward bias, resulting in large turn-off times (seconds) as the junction needs to be fully depleted before a low reverse bias current is obtained (Figure S5, Supporting Information).[16,17] Consequently, iontronic diode bridge performance is far from ideal and exhibits a transient state immediately after switching the input polarity as both sets of diodes are conducting.[34] This leads to a significant drop, or sometimes even a reversed peak, of the output voltage. Subsequently, this results in a discontinuity of the delivery of an ionic current through the OEIP, which is applied to the output terminals (i.e., the bridge load). We therefore designed a new iontronic diode bridge circuit, incorporating

**ADVANCED
SCIENCE NEWS**
www.advancedsciencenews.com

**ADVANCED
MATERIALS
TECHNOLOGIES**
www.advmattechnol.de

Figure 5. Smoothing of output in ionic diode bridge circuit. A) Circuit schematic for an ionic diode bridge, incorporating a smoothing capacitor. The faded diodes are reverse biased. The blue line represents the ionic current through the circuit for the applied bias, and the dashed line the transient ionic current through the capacitor during charge and discharge. B) Rendering of the circuit as manufactured. The labels indicate D, diode (one of four); R, resistor (OEIP); C, capacitor; In$_1$ and In$_2$, input electrodes. The white scale bar represents 1 mm. In order to minimize resistance, the capacitor and output resistor were placed as close as possible to each other. C) Ionic current rectification of an input square wave (red), without (purple) and with (green) smoothing capacitor. D) Detailed view of the smoothing effect, with and without inclusion of the capacitor.

the ionic capacitor (electrode size of 4.4 mm^2) connected in parallel with the output OEIP, to act as a smoothing capacitor (Figure 5A,B). Smoothing capacitors are commonly applied to electronic diode bridge circuits to stabilize the full-wave rectified output voltage. In its steady-state, the capacitor of the iontronic diode bridge is fully charged and most of the current passes through the OEIP. When the input polarity is reduced or switched, the capacitor will discharge. Part of the discharge current of the capacitor will pass through the OEIP, thus maintaining (smoothing) the output current, and the remaining discharge current passes through the "open" diodes. When the reverse-biased diodes are depleted, the current through the forward-biased diodes will continue to pass through the OEIP, the capacitor will recharge, and the circuit will again approach a steady-state condition.

We tested the smoothing effect of this improved iontronic diode bridge by applying a ±0.8 V square-wave input with a period of 600 s and recording the output voltage over the OEIP with and without the capacitor connected (Figure 5C). At steady-state, the output voltage reached 700–800 mV, depending on input polarity. However, without the capacitor, the output voltage shows negative peaks around −400 mV generated immediately after each switch of the input polarity. With the capacitor, the output voltage gradually decreases after each switch but never reaches below +600 mV and the lowest value is reached with a delay of about 20 s with respect to the switch in input voltage (Figure 5D). As a result, the output voltage was significantly higher with the capacitor during the first ≈15 s after each switch of the input polarity. The recovery time to steady-state was similar in both cases. The addition of the ionic capacitor thus smooths the output voltage of the circuit and has an overall positive effect on the continuity of ion delivery through the OEIP.

In conclusion, this work reports a PEDOT:PSS-based ionic capacitor and its implementation in an iontronic circuit. In a sense, the ionic capacitor is an inverted electronic electro-

chemical supercapacitor, with an electronically conducting core, two electronically and ionically active electrodes, and two electrolyte conductors. The ionic capacitor shows several typical capacitor performance parameters, such as a linear variation of the capacitance value versus the electrode area/volume and an overall linear galvanostatic charge/discharge characteristics (here recorded at up to 3.6 A cm^{-3}). The maximum specific capacitance (capacitance per total volume of electrodes) of this PEDOT:PSS-based ionic capacitor is similar to the graphene oxide–based ionic capacitor previously reported[19] (7.7 F cm^{-3} at 12.5 mV s^{-1} in present study vs 7.5 F cm^{-3} at 1 mV s^{-1} in ref. [19]) but is significantly less affected by high scan rates (3.52 F cm^{-3} at 800 mV s^{-1} in present study vs 0.4 F cm^{-3} at 500 mV s^{-1} in ref. [19]). The mixed electronic-ionic nature of PEDOT:PSS[35] could be a possible reason for the difference, as this should facilitate higher ion conductivity than electrolyte-filled porous graphene oxide.

The capacitors studied in the first part of this work are, in structure and function, equivalent to two electrochemical supercapacitors in series: two stacks of conjugated polymer electrode—electrolyte—conjugated polymer electrode. However, this equivalence fails once the capacitor is integrated into more advanced iontronic circuitry, as (iontronic) components then would connect between the two electrolytes (see Figure S6, Supporting Information). Further, in contrast to ordinary capacitors with electron conducting terminals, an ionic capacitor can be directly incorporated into iontronic circuitry, here as a smoothing capacitor for a full-wave diode rectifier, without the need of additional electrochemical electrodes to provide for electron–ion conversion. This suggests that the ionic capacitor is a valuable asset in the iontronics toolbox and can facilitate more advanced iontronic circuitry in the future. For instance, improvement in smoothness of the output signal could be beneficial for neuronal direct current stimulation applications,[36] in electroosmotic pumps[37] and electrokinetic devices.[38]

Experimental Section

Device and Circuit Manufacturing: *Preparation of qPVBC*: The procedure for obtaining the quaternized polyammonium was as earlier reported.[17]

Manufacturing of the Devices: The general materials and procedures for manufacturing of the device were reported before.[34] Briefly, a circular 4″ substrate of polyethylene terephthalate (PET) with a thin film of PEDOT:PSS (AGFA-Gaevart Orgacon F-350) was patterned by photolithography with a Karl Suss MA/BM 6 mask aligner followed by a plasma etch of CF_4/O_2 to define electrodes, cation-selective channels, and capacitor area. To create the cation-selective materials, a protective layer was patterned and the substrate was treated with sodium hypochlorite (0.5 vol%) for 10 s to render the exposed PEDOT:PSS electronically inactive, while retaining the iontronic properties of PSS. The capacitor PEDOT:PSS electrodes was connected by painting carbon paste with a brush into a 2.5 µm SU8 (SU8-2002, MicroChem) defined well. The anion-selective material (qPVBC) was applied through spin coating and defined using photolithography and a CF_4/O_2 plasma etch. The device was then encapsulated with a 10 µm SU8-layer (SU8-2010, MicroChem) and contacts were covered with silver ink (AG500, Applied Ink Solutions).

Capacitor Characterization: The capacitor characterizations were made on a Biologic SP200 potentiostat. Patterned PEDOT:PSS electrodes, > 4 × larger than the largest capacitor electrode and with extra PEDOT:PSS deposited (Heraeus Clevios PH1000 cross-linked with (3-glycidyloxypropyl) trimethoxysilane) were used to connect to the capacitor.

Circuit Measurements: The full circuit measurements were made on a Keithley 2602A SourceMeter at 20 Hz with NPLC set at 2. The Keithley was controlled and data collected using a custom LabVIEW program. 0.1 M KCl was used as electrolyte. The output voltage was measured using patterned PEDOT:PSS electrodes located in close proximity to the OEIP channel.

PEDOT:PSS Electrode Thickness: Parts of the PEDOT:PSS film on pristine AGFA-Gaevart Orgacon F-350 were removed by gently rubbing using a wet cleanroom swab. Following cleaning with acetone and water, the resulting step in the film were measured using an optical profilometer (Sensofar PLu Neox).

Supporting Information

Supporting Information is available from the Wiley Online Library or from the author.

Conflict of Interest

The authors declare no conflict of interest.

[1] G. Tarabella, F. M. Mohammadi, N. Coppede, F. Barbero, S. Iannotta, C. Santato, F. Cicoira, *Chem. Sci.* **2013**, *4*, 1395.

[2] J. Rivnay, R. M. Owens, G. G. Malliaras, *Chem. Mater.* **2014**, *26*, 679.

[3] G. Lanzani, *Nat. Mater.* **2014**, *13*, 775.

[4] G. G. Malliaras, *Biochim. Biophys. Acta, Gen. Subj.* **2013**, *1830*, 4286.

[5] D. T. Simon, E. O. Gabrielsson, K. Tybrandt, M. Berggren, *Chem. Rev.* **2016**, *116*, 13009.

[6] H. Chun, T. D. Chung, *Annu. Rev. Anal. Chem.* **2015**, *8*, 441.

[7] J. Isaksson, P. Kjaell, D. Nilsson, N. D. Robinson, M. Berggren, A. Richter-Dahlfors, *Nat. Mater.* **2007**, *6*, 673.

[8] I. Uguz, C. M. Proctor, V. F. Curto, A.-M. Pappa, M. J. Donahue, M. Ferro, R. M. Owens, D. Khodagholy, S. Inal, G. G. Malliaras, *Adv. Mater.* **2017**, *29*, 1701217.

[9] Nazrin Abdullayeva, Mehmet Sankir, *Materials* **2017**, *10*, 586.

[10] A. Williamson, J. Rivnay, L. Kergoat, A. Jonsson, S. Inal, I. Uguz, M. Ferro, A. Ivanov, T. A. Sjöström, D. T. Simon, M. Berggren, G. G. Malliaras, C. Bernard, *Adv. Mater.* **2015**, *27*, 3138.

[11] A. Jonsson, S. Inal, L. Uguz, A. J. Williamson, L. Kergoat, J. Rivnay, D. Khodagholy, M. Berggren, C. Bernard, G. G. Malliaras, D. T. Simon, *Proc. Natl. Acad. Sci. U. S. A.* **2016**, *113*, 9440.

[12] D. T. Simon, S. Kurup, K. C. Larsson, R. Hori, K. Tybrandt, M. Goiny, E. W. H. Jager, M. Berggren, B. Canlon, A. Richter-Dahlfors, *Nat. Mater.* **2009**, *8*, 742.

[13] A. Jonsson, Z. Song, D. Nilsson, B. A. Meyerson, D. T. Simon, B. Linderoth, M. Berggren, *Sci. Adv.* **2015**, *1*, e1500039.

[14] O. J. Cayre, T. C. Suk, O. D. Velev, *J. Am. Chem. Soc.* **2007**, *129*, 10801.

[15] J. H. Han, K. B. Kim, H. C. Kim, T. D. Chung, *Angew. Chem., Int. Ed.* **2009**, *48*, 3830.

[16] J.-H. Han, K. B. Kim, J. H. Bae, B. J. Kim, C. M. Kang, H. C. Kim, T. D. Chung, *Small* **2011**, *7*, 2629.

[17] E. O. Gabrielsson, K. Tybrandt, M. Berggren, *Lab Chip* **2012**, *12*, 2507.

[18] K. Tybrandt, K. C. Larsson, A. Richter-Dahlfors, M. Berggren, *Proc. Natl. Acad. Sci. U. S. A.* **2010**, *107*, 9929.

[19] S. T. Martin, A. Akbari, P. Chakraborty Banerjee, A. Neild, M. Majumder, *Phys. Chem. Chem. Phys.* **2016**, *18*, 32185.

[20] S. Ghosh, O. Inganäs, *Electrochem. Solid-State Lett.* **1999**, *3*, 213.

[21] Y. Liu, B. Weng, J. M. Razal, Q. Xu, C. Zhao, Y. Hou, S. Seyedin, R. Jalili, G. G. Wallace, J. Chen, *Sci. Rep.* **2015**, *5*, 17045 EP.

[22] T. Cheng, Y.-Z. Zhang, J.-D. Zhang, W.-Y. Lai, W. Huang, *J. Mater. Chem. A* **2016**, *4*, 10493.

[23] Y. Li, G. Ren, Z. Zhang, C. Teng, Y. Wu, X. Lu, Y. Zhu, L. Jiang, *J. Mater. Chem. A* **2016**, *4*, 17324.

[24] X. Li, J. Shao, S.-K. Kim, C. Yao, J. Wang, Y.-R. Miao, Q. Zheng, P. Sun, R. Zhang, P. V. Braun, *Nat. Commun.* **2018**, *9*, 2578.

[25] G. Sonmez, C. K. F. Shen, Y. Rubin, F. Wudl, *Angew. Chem., Int. Ed.* **2004**, *43*, 1498.

[26] J. M. D'Arcy, M. F. El-Kady, P. P. Khine, L. Zhang, S. H. Lee, N. R. Davis, D. S. Liu, M. T. Yeung, S. Y. Kim, C. L. Turner, A. T. Lech, P. T. Hammond, R. B. Kaner, *ACS Nano* **2014**, *8*, 1500.

[27] C. M. Proctor, J. Rivnay, G. G. Malliaras, *J. Polym. Sci., Part B: Polym. Phys.* **2016**, *54*, 1433.

[28] A. V. Volkov, K. Wijeratne, E. Mitraka, U. Ail, D. Zhao, K. Tybrandt, J. W. Andreasen, M. Berggren, X. Crispin, I. V. Zozoulenko, *Adv. Funct. Mater.* **2017**, *27*, 1700329.

[29] K. Tybrandt, I. V. Zozoulenko, M. Berggren, *Sci. Adv.* **2017**, *3*, eaao3659.

[30] S. Fabiano, N. Sani, J. Kawahara, L. Kergoat, J. Nissa, I. Engquist, X. Crispin, M. Berggren, *Sci. Adv.* **2017**, *3*, e1700345.

[31] M. Hayyan, F. S. Mjalli, M. A. Hashim, I. M. AlNashef, T. X. Mei, *J. Ind. Eng. Chem.* **2013**, *19*, 106.

[32] E. O. Gabrielsson, M. Berggren, *Biomicrofluidics* **2013**, *7*, 064117.

[33] E. O. Gabrielsson, K. Tybrandt, M. Berggren, *Biomicrofluidics* **2014**, *8*, 064116.

[34] E. O. Gabrielsson, P. Janson, K. Tybrandt, D. T. Simon, M. Berggren, *Adv. Mater.* **2014**, *26*, 5143.

[35] E. Stavrinidou, P. Leleux, H. Rajaona, D. Khodagholy, J. Rivnay, M. Lindau, S. Sanaur, G. G. Malliaras, *Adv. Mater.* **2013**, *25*, 4488.

[36] G. Y. Fridman, C. C. Della Santina, *IEEE Trans. Neural Syst. Rehabil. Eng.* **2013**, *21*, 319.

[37] A. Brask, D. Snakenborg, J. P. Kutter, H. Bruus, *Lab Chip* **2006**, *6*, 280.

[38] P. G. Erlandsson, N. D. Robinson, *Electrophoresis* **2011**, *32*, 784.